NIH Public Access
Author Manuscript
*Top Magn Reson Imaging*. Author manuscript; available in PMC 2012 April 4.

Published in final edited form as:
*Top Magn Reson Imaging*. 2010 April ; 21(2): 129–138. doi:10.1097/RMR.0b013e31821e56c2.

# Multiparametric MR Imaging of Brain Disorders

**Ona Wu, PhD**[1], **Rick M Dijkhuizen, PhD**[2], and **Alma Gregory Sorensen, MD**[1]

[1]Athinoula A Martinos Center for Biomedical Imaging, Department of Radiology, Massachusetts General Hospital, Charlestown, MA 02129, USA [2]Biomedical MR Imaging and Spectroscopy Group, Image Sciences Institute, University Medical Center Utrecht, Utrecht, 3584 CM, The Netherlands

## Abstract

Magnetic resonance imaging (MRI) has been shown to improve the diagnosis and management of patients with brain disorders. Multiparametric MRI offers the possibility of noninvasively assessing multiple facets of pathophysiological processes that exist simultaneously, thereby further assisting in patient treatment management. Voxel-based analysis approaches, such as tissue theme mapping, have the benefit over volumetric approaches in being able to identify spatially heterogeneous co-localized changes on multiple parametric MR images that are not readily discernible. Tissue theme maps appear to be a promising tool for integrating the plethora of novel imaging contrasts that are being developed for the non-invasive investigation of the different stages of disease progression into easily interpretable maps of brain injury. We describe here various implementations for combining multiparametric imaging and their merits in the evaluation of brain diseases.

### Keywords

MRI; Multiparametric; Multimodal; models; brain disorders; predict

## Introduction

Magnetic resonance imaging (MRI) plays important roles in the diagnosis and prognosis of patients with brain disorders ranging from acute conditions such as stroke and traumatic brain injury (TBI) to chronic illnesses such as multiple sclerosis and epilepsy. As a step towards personalized medicine, many have speculated that imaging can be used to develop treatment plans for these patients that take into account individual variation[1–5]. MRI also offers the potential of noninvasive longitudinal monitoring of disease progression, for example in the case of brain tumors when repeated biopsies can be burdensome. MRI has frequently been speculated to provide potential biomarkers for monitoring the effects of therapies at both pre-clinical and clinical stages, and for optimizing patient selection in clinical trials of novel drugs [6]. Further, some investigators have advocated the use of imaging as a surrogate endpoint for long term outcome in clinical trials due to the ease of translation of results between pre-clinical and clinical settings[7].

Corresponding Author: Ona Wu, Athinoula A Martinos Center for Biomedical Imaging, Department of Radiology, Massachusetts General Hospital, Charlestown, MA 02129, Telephone: 617-643-3878, Fax: 617-643-3939, ona@nmr.mgh.harvard.edu.
Address for Reprints: Same as above

NIH-PA Author Manuscript
NIH-PA Author Manuscript
NIH-PA Author Manuscript

NIH-PA Author Manuscript

NIH-PA Author Manuscript

NIH-PA Author Manuscript

## Multimodal MRI

Combining multiple imaging contrasts that reflect different aspects of pathophysiological processes may provide additional insight over what can be gleaned from a single imaging parameter. In addition, individual MRI parametric maps typically present single snapshots in time of disease processes that are highly dynamic. For example, in acute stroke patients, to better assess tissue viability and potential recovery after therapeutic intervention in regions of reduced cerebral blood flow (CBF), extra data on changes in cerebral blood volume (CBV) (e.g. whether it is reduced[8] or elevated[9]) may be critical.

There are several methods for multimodal imaging analysis. Some involve evaluating diverse imaging datasets that are typically acquired at the same imaging session, while other approaches may concentrate on the investigation of longitudinally acquired single parametric maps. One strategy for analyzing multiparametric data involves extracting relevant features, such as volume or signal intensity, and then performing statistical tests or modeling on those factors. Figure 1 demonstrates such an approach in which one compares lesion volumes between acute trace-weighted diffusion-weighted MRI (DWI) and peak time of the deconvolved residue function (Tmax) of perfusion-weighted MRI (PWI). This can be followed, according to one's hypothesis, by statistical tests such as analysis of variance to determine if there exists a difference in volumes between groups, or multivariate regression to predict an outcome variable. Region of interest (ROI) analysis can also be performed in which one compares signal intensity in different patient cohorts, e.g. treated or non-treated. These volumetric regional approaches have been used to investigate several brain disorders ranging from acute stroke[10–12], brain tumors[13], migraine[14], multiple sclerosis[15], dementia[16], CADASIL[17], Alzheimer's disease[18] and epilepsy[19, 20] to name a few. A benefit of a volumetric or ROI based methodology is that one does not need spatially aligned datasets and can concentrate on particular features of interest, excluding *a priori* noisy data. However, as the number of quantitative novel MRI contrasts continues to increase, thereby increasing the amount of images to interpret, readily identifying regions of abnormal tissue in multitude of images would be cumbersome and unfeasible in acute clinical settings.

Another strategy for performing multimodal analysis is a voxel-wise approach (see Figure 2). In this technique, one transforms quantitative imaging values for each voxel $<i,j,k>$ from each parametric map, $X_{ijk,1\ldots N}$, to create a single new imaging map $T$ for which the value at each voxel $<i,j,k>$ is a function, $\Im$, of $N$ parameters. This function may either be a linear or nonlinear. Similar to the volumetric approach, feature selection must also be performed for the voxel-based approach, however, in this case it primarily involves choice of which imaging parameters to combine. The benefit of this method is that one can investigate voxel-wise changes that may otherwise be obscured when taking an aggregate value in an ROI (e.g. mean or median value). This heterogeneity has been shown to occur for water self-diffusivity or apparent diffusion coefficient (ADC) [10, 21–23], and other parameters such as CBF and CBV, which not only vary by tissue pathology[24–28] but also by tissue type. Further, it may be the co-localized changes in these parameters that can provide the best insight into which tissue is most severely injured and which tissue is most likely to respond to therapy. Indeed, the heterogeneity in the pathophysiology of human stroke is thought by some to account for the limited success of therapeutic interventions[29, 30]. Furthermore, integration of lesion location with lesion size was found to create a better estimator of clinical outcome than volume alone[31]. This weighting of location and lesion load is exactly what talented clinicians do intuitively at the bedside for a variety of brain disorders as they look at the scans of a given patient. Therefore a single image that combines a myriad of potential markers of tissue viability into a simple imaging signature or theme map that can be easily understood and used to assess tissue status accurately and objectively would be an ideal tool for quantifying the impact of new therapeutic interventions, and possibly for

NIH-PA Author Manuscript

NIH-PA Author Manuscript

NIH-PA Author Manuscript

assisting the clinical decision-making process. One disadvantage of a voxel-wise approach is that accurate co-registration of the data is necessary. Fortunately, several algorithms and software exist for performing co-registration (e.g. MNI Autoreg, McConnell Brain Imaging Center, Montreal Neurological Institute[32]; FLIRT, FMRIB Centre, Department of Clinical Neurology, University of Oxford[33, 34]; Automatic Image Registration, Laboratory of Neuro Imaging, UCLA[35, 36]), and MRI manufacturers have developed automatic MRI slice positioning protocols (e. g., AutoAlign) that enable the precise and consistent alignment of scans among different individuals and repeated imaging of the same individidual[37, 38].

Early advances in terms of integration of multiple MRI datasets to create a tissue theme or signature map have been made in the field of cerebral ischemia. However, there has been increasing interest in the use of theme maps in other brain diseases. We will use primarily the framework of cerebral ischemia and brain tumors to discuss some of the approaches developed for theme map calculation. However, these approaches can readily be extended to other brain diseases.

## Tissue Theme Map Calculation

### Inputs

The imaging data used to create tissue signature models depends on several factors such as the application, the disease to be studied and pertinent collected imaging modalities. Therefore detailed descriptions of particular MRI parametric maps that can be used, e.g. DWI and PWI, will not be discussed in this article. However, we do note that whichever maps are used, one important consideration for theme map generation is whether one should use a “weighted” image (i.e. raw acquired MRI signal intensity data) or a quantitative “parametric” map (i.e. derived maps calculated from raw acquired data). Both “weighted” imaging parameters and “parametric” maps have been found to perform with varying degrees of success, though the use of surface coils in data acquisition have often precluded the use of weighted images due to image inhomogeneities that can lead to incorrect classification. Most techniques normalize imaging parameters with respect to a reference tissue that is stable across scan sessions and subjects, e.g. normal contralesional white matter. This is useful particularly for cross-subject comparisons. Normalization is typically performed as a pre-processing step on the input data prior to training the model or on a post hoc basis to standardize the output results. The risk with this approach is that it assumes the differences between “weighted-images” are linear scaling effects uniformly spatially distributed, which are often not the case, especially when multi-channel array head coils are used. Non-uniformity correction prior to normalization can compensate for some of these artifacts, but not completely. Therefore, it would be preferable to generate models with parametric maps if the equivalent information was available, e.g. T2-maps instead of T2-weighted maps. One of the drawbacks of parametric maps is that longer acquisition times are often required to obtain the data necessary for calculating the quantitative maps.

### Models

Tissue theme map calculation can be broadly classified into two categories: supervised or unsupervised algorithms. Unsupervised algorithms use the inherent data heterogeneity within a given dataset to automatically determine distinct features between different tissue classes, e.g. infarcted versus non-infarcted tissue. Supervised algorithms, in contrast, “learn” to distinguish tissue classes using training sets that are representative of data acquired from patients with the same disorder in which the state of tissue injury is known, e.g. measured with histopathology or on follow-up imaging. In supervised learning algorithms, the outcome states are *a priori* determined and a training dataset is used to develop a model that minimizes misclassification rates in the training data. With supervised algorithms, one needs

NIH-PA Author Manuscript

NIH-PA Author Manuscript

NIH-PA Author Manuscript

to be careful not to "overfit" on the training data in order for the model to be applicable to other datasets. "Overfitting" of an algorithm typically occurs when one uses too many variables, such that the variables fit the noise of the particular training data set rather than the physiological process one is seeking to model. The over-fitted algorithm will typically do very well on its training data set, but poorly on new data sets. Consequently, results of supervised learning algorithms need to be cross-validated on an independent dataset in order to evaluate the models' generalizability. This is used to avoid bias that would otherwise occur if the model's performance were evaluated on the same data that was used to train the model. Despite the extra overhead, a benefit of a supervised approach is that the output is typically well-defined. With unsupervised algorithms that automatically segment the tissue into different classes or clusters, as additional parameters are added, the model results may become more difficult to interpret [39], or generate clusters that might not have a readily discernible biological meaning. On the other hand, unsupervised algorithms do not need a training dataset and hence are not concerned with overfitting a model to the training data. We will broadly cover examples of both approaches. It should be noted that learning algorithms are an active area of investigation among the machine learning community. Given the breadth and variety of available algorithms, the reader is referred to Duda [39] or Bishop [40] for more details.

**Supervised Learning Algorithms—**One of the earliest examples of theme map generation using imaging for improving our understanding of disease progression was developed by Welch et al [22]. Based on data from experimental stroke literature [41, 42], Welch et al formulated an MR-based theme map characterizing the stages of lesion evolution in cerebral ischemia. Six signatures of tissue stages were identified that represented (A) normal tissue with normal ADC and normal T2-weighted MRI (T2WI), (B) tissue that may or may not be salvageable with reduced ADC and normal T2WI, (C) tissue at high risk of necrosis with reduced ADC and elevated T2WI, (D) tissue that is transitioning to necrosis with normal ADC and elevated T2WI, (E) tissue that is irreversibly necrotic with elevated ADC and elevated T2WI, and (F) tissue with established cell necrosis with elevated ADC and normal T2WI. This approach combined both *a priori* suppositions about biology and broad clustering of imaging parameters. They tested this tissue signature model, derived from the experimental stroke literature, on MRI data collected from eight patients (scanned between 24 to 116 h post-stroke onset). Upper and lower threshold values for ADC and T2WI were chosen based on normal gray and white matter tissue values in the contralateral hemisphere, and used to create thresholds for tissue classification. The thresholds were selected using an iterative supervised approach (Figure 3A). Voxels for which the coregistered values fell into a particular region were labeled accordingly (Figure 3B) and mapped to create a theme map displaying the spatial distribution of the tissue signatures (Figure 3D). Clearly evident is the heterogeneity of the distribution of the signatures in the stroke patient in Figure 3. Welch et al noted that the B signature, which often surrounded signatures C and D, represents tissue that may still be salvageable, while C and D show tissue that is at high risk or transitioning to necrosis. This work demonstrated that using multiparametric maps provide images that correlate with hypothesized stages of disease evolution that would not be detectable using standard ROI analysis approaches, since it was the interaction of the two parameters that were important for staging the tissue's pathological state.

A similar multiparametric approach was used by Moffat et al to analyze a single imaging modality, ADC, across multiple time points for stratification of brain tumor response to therapy[43]. Moffat et al created functional diffusion maps (fDM) that mapped changes on co-registered ADC maps acquired in patients with malignant brain tumor, before and three weeks after initialization of therapy (radiation and/or chemotherapy). Patients were assigned a green signature if there was no change in ADC, a blue signature if ADC decreased (assumed to be an indication of increased cellularity or water redistribution without

NIH-PA Author Manuscript

NIH-PA Author Manuscript

NIH-PA Author Manuscript

significant cell lysis) and a red signature if ADC increased (representing cells undergoing necrosis or apoptosis). Thresholds for whether a change in ADC was significant or not, were determined from a training set composed of data from five other patients. The green signature was thought to represent tissue resistant to therapy, while the other signatures were associated with partial response to therapy as verified on follow-up imaging four weeks after therapy. The percent of the total volume that was assigned red or blue signatures was found to be 100% sensitive and specific in identifying which patients would exhibit partial recovery from those with stable or progressive disease, in a group of 20 patients, at only 3 weeks into therapy. A later study in a cohort of 60 patients with high grade glioma receiving radiotherapy, demonstrated that fDM was also predictive of overall survival, with patients exhibiting increases in ADC to be most likely to be alive at 1 year[44]. Another study used the same approach to map changes in relative CBF and CBV values (normalized with respect to contralesional white matter) before and after therapy in 44 high grade glioma patients undergoing radiotherapy, generating parametric response maps (PRM), a generalized form of the fDM [45]. The PRM was found to be more predictive at 1 and 3 weeks of survival at 1 year than examining percent change in CBF and CBV using ROI analysis in the tumor volume. This was attributed to the heterogeneity of blood flow and blood volume between normal gray and white matter and diseased tumor tissue which ROI analysis obscured. In addition to early prediction of lack of effectiveness of therapy, a multiparametric spatial mapping technique can potentially be used for guiding therapies that can be targeted at specific tissue [46].

Wu et al used a generalized linear model (GLM) to predict tissue infarction for stroke patients given standard of care (N=14) [47], that is non-thrombolytic or catheter-based therapy. Tissue outcome was modeled as a binary variable, for which 1 represented infarcted tissue and 0 represented non-infarcted tissue in the training data set. The output of this algorithm was the probability, P, of tissue belonging to the infarcted or non-infarcted class given acute imaging presentation. P was a combination of input maps, **x**, which consisted of acute DWI, ADC, T2WI, CBF, CBV and MTT normalized to contralateral tissue on a voxel-wise basis utilizing a logistic function:

$$P(\mathbf{x})=\frac{1}{1+e^{-\eta(\mathbf{x})}}. \quad \text{(Equation 1)}$$

The predictor, η(x), was a linear function of x:

$$\eta(\mathbf{x})=\beta^{T}\mathbf{x}+\alpha, \quad \text{(Equation 2)}$$

for which β was a vector of calculated coefficients and α was the bias or intercept term. The coefficients α and β that characterized the GLM were calculated from the training data group using an iterative re-weighted least squares algorithm. The calculated coefficients were then used to make predictions for new datasets using Equation 1 and Equation 2. Since additional terms may produce a better mathematical fit that yields no additional biological insight by overfitting to the training data, the decision to include additional parameters or not was based on the Akaike Information Criterion (AIC), a measure that was a function of both training error and complexity [40]. Due to the limited number of patients in the study, instead of cross-validation in which a second dataset is used to evaluate the generalizability of the model, the predictive performance was evaluated using jack-knifing or a leave-one-out approach in which the coefficients for each patient were calculated using data from the other patients in the group as training data [48]. This approach was found to more accurately predict tissue infarction by follow-up than any single imaging modality when thresholding the probability map at its optimal operating point. An example risk map generated using this

NIH-PA Author Manuscript

NIH-PA Author Manuscript

NIH-PA Author Manuscript

approach is shown in Figure 4 along with input imaging parameters. Rather than using a hard classification of tissue with a probability greater than a single threshold, e.g. 50%, as expected lesion (e.g. a binary mask consisting of values of 0 or 1), one can also interpret the maps as the likelihood of tissue dying without interventional therapy (e.g. a continuous variable from 0 to 100%). An alternate interpretation is that the output represents degree of existing tissue injury at the time of imaging. For example, for Figure 4 one sees that the infarction risk map shows a heterogeneous region of injured tissue, with regions of higher infarction risk (red) matching areas of low ADC and increased trace DWI, consistent with regions of the infarcted core. Notably the predicted lesion is smaller in size than the MTT abnormality, often assumed to represent potentially salvageable tissue, but corresponds well with tissue that was found to be infarcted on follow-up imaging. The probability values in these regions are notably lower than in the "core" region. Again, if one used just a simple volumetric mismatch approach between acute DWI and acute MTT, the heterogeneous distribution of tissue risk would have been obscured.

Another benefit of the GLM approach is that the results have a straightforward interpretation independent of the number of imaging input parameters, namely the probability that the tissue will be classified as abnormal. Figure 5 shows an example output including Tmax as an additional parameter. The output appears very similar to Figure 4 and can be interpreted in the same manner. Both overlays are displayed showing only tissue with P values > 50%. It appears that for the particular patient in Figure 4, the inclusion of Tmax did not significantly change lesion classification despite the volume with abnormal Tmax in this patient being much larger than the areas with abnormal MTT and predicted high infarction risk. However, in a study of 80 patients, the inclusion of Tmax, on average, significantly improved the predictive performance of the model over using the original six parameters[49]. The GLM approach was also used to evaluate differences between patients given standard of care (N=11) and those given thrombolytic therapy (N=27) [50]. The authors showed that patients who were treated with thrombolytic therapy and experienced early reperfusion had smaller lesion volumes than were predicted by the GLM, resulting in lower accuracy than in those patients not given thrombolytics. This suggests that the GLM can be used to evaluate therapeutic efficacy of new drugs by comparing actual outcome with expected outcome. Deviations from predicted outcome would be an indication of the treatment affecting its biologic target, which for certain diseases may be regionally specific, e.g. neuroprotective drugs that selectively targets gray matter in potentially salvageable tissue around a core of infarcted tissue.

One limitation of the GLM is the assumption of linearity, which may not be correct for all input parameters. For example, both abnormally high ADC values, and abnormally low ADC values, are predictive of tissue infarction [10]. Both low and high CBV have also been observed in the acute stage in areas that became infarcted on follow-up [51]. Therefore, models such as generalized additive models (GAM) [52], the functional form of which is derived from their data, have been speculated to potentially provide a better estimate of infarction state over models that assume an a priori linear dependence, such as the GLM [53].

Rose et al developed a parametric normal classifier [54] to predict tissue outcome in which the output was represented as two classes: infarcted or non-infarcted[55]. The input consisted of an eight-parameter vector **X** in voxels from abnormal MTT tissue: DWI, relative DWI, CBF, relative CBF, CBV, relative CBV, MTT, and relative MTT. Relative values were calculated with respect to contralateral hemisphere. The model was trained on 10 datasets to produce probability distribution functions assuming normal distributions, and validated on 7 datasets for the purposes of cross-validation. For the 10 patients used to develop the training data, jack-knifing was used for validation. These models were found to be able to predict lesion growth. This approach was also used for tissue classification using ADC, CBF index, T2,

NIH-PA Author Manuscript

NIH-PA Author Manuscript

NIH-PA Author Manuscript

and proton density imaging data from an experimental stroke model, however in this case there were 3 output classes consisting of abnormal and normal tissue and cerebral spinal fluid (CSF) [56].

There are also approaches that allow for improved prediction but at the cost of more complexity in the modeling of the output as a function of the input images. The hierarchical mixture of experts (HME) is a tree-structured architecture consisting of gating and expert networks [57], the gating networks of which select the appropriate expert based on the input data. The HME was shown to improve prediction of tissue outcome compared to the GLM [58]. Non-parametric approaches such as k-nearest neighbors (kNN) algorithm have been proposed for combining multivariate data for both stroke[56, 59] and for tumor patient evaluation [60]. The kNN algorithm, which does not have a previous assumption regarding data distribution, classifies each new input vector according to the label of its k-nearest neighbors in the training data, in which distance is often measured with a Euclidean metric. For a human stroke study (N=14) [59], the label was “infarcted” or “non-infarcted” tissue on follow-up imaging (more than 5-days from onset), while for the tumor study in grade IV tumor patients (N=26) [60], the label was “enhanced” or “non-enhanced” tissue on post-radiotherapy imaging (within one month of conclusion of therapy) for tissue that was originally non-enhancing. The number of labels can be more than two, as was the case for the experimental stroke study for which the labels were normal, abnormal, or CSF [56]. For predicting tissue infarction in stroke patients, kNN was shown to perform similarly to the GLM for input vectors consisting of normalized acute DWI, ADC, T2WI, CBF, CBV and MTT [59], using a jack-knifing for cross-validation. The stroke study [59] used features that were determined by previous studies to be useful [47]. For predicting tissue enhancement in tumor patients, the input vector consisted of 38 features including fractional anisotropy, ADC, CBV, contrast agent bolus curve shape parameters, and proton spectroscopic data (spectral heights and width) acquired 2 weeks before initiation of therapy. Here, the authors weighted the features using genetic optimization due to the known sensitivity of the kNN to parameter scaling and noise from numerous features included in the model. The genetic algorithm demonstrated that using only 7 of the 38 features could produce an accurate prediction of post-treatment contrast-enhancement, using a leave-one-out approach for validation.

**Unsupervised Learning Algorithms—**An example of a fully unsupervised classification approach is the K-Means (KM) algorithm. The basic KM algorithm clusters voxels by minimizing intracluster distance metrics, in which the number of clusters, K, is *a priori* specified. Distance metrics that have been typically used include Euclidean or Mahalanobis distance metric. KM has been applied to both lesion prediction in experimental stroke models [61] and differentiating benign and malignant lesions in human patients[62]. Carano et al showed in an experimental stroke model that using KM to cluster acute quantitative T2 maps, ADC, relative CBF and proton density signal into three classes (CSF, normal and abnormal tissue), produced results that better correlated with post-mortem histological findings than results based on a simple ADC threshold. Srinivasan et al used KM to segment ADC into two (high, low) or three (high, low, intermediate) clusters in patients with head and neck lesions and found a statistically significant difference in the low clusters between malignant and benign lesions [62].

A limitation of KM clustering is that it requires that the number of classes (K) is established prior to processing. The Iterative Self Organizing Data Analysis (ISODATA) technique extends the KM algorithm by dynamically adjusting the number of classes based on distance metrics between centers of different clusters (inter-cluster) and between members of the same cluster (intra-cluster) [63, 64]. Clusters with centers that are relatively close will be combined, while a single cluster with members that are relatively far apart will be split. This

NIH-PA Author Manuscript

NIH-PA Author Manuscript

NIH-PA Author Manuscript

is repeated until convergence measured by cluster variances within a threshold is achieved or an iteration limit is reached. Because of its lack of reliance of a priori determined number of clusters, ISODATA can be used to show heterogeneity of the values of a parametric map at a single time point. Figure 6 illustrates ISODATA classification procedures. Nagesh et al used an ISODATA approach to combine four trace DWI data sets acquired at b-values of 0, 300, 600 and 900 s/mm2 to examine heterogeneity of ADC in nine stroke patients imaged within 10h of stroke onset [21]. They found multiple signatures within ischemic tissue that corresponded to reduced, pseudo-normal and elevated ADC. ISODATA was also used to combine data from multiple parametric maps. Jacobs et al[65] used this approach to characterize tissue over time in ten stroke patients scanned at three time points: acute (<= 12 hours), subacute (3 to 5 days), and chronic (3 months). Imaging parameters to the ISODATA segmentation algorithm consisted of two T2WI acquired at echo times of 30 and 90 ms, 1 T1 weighted image (T1WI), and two DWI acquired at b-values of 600 and 1000 s/mm$^2$. The volume of ischemic tissue damage, as determined by acute ISODATA, was highly correlated with the follow-up clinical outcome of the patient. Moreover, features that were detectable on the combined ISODATA map were not evident on the individual DWI, ADC or T2 maps. This suggests that ISODATA can be used to accurately and non-invasively characterize the evolution of ischemic tissue damage. Another study found that the acute ISODATA determined lesion correlated with the acute PWI abnormality in stroke patients seen within 36 h from stroke onset (N=11) [66].

One limitation of ISODATA is the need for post-hoc interpretation of the clusters. Soltanian-Zadeh et al have proposed an extension to ISODATA that orders the clusters fo standardization of output results [67]. The approach consists of creating an MRI score that reflects the Euclidean distance between each ISODATA cluster, *i*, and normal reference tissue signature, $ED_{i,\text{Normal}}$, and CSF signature, $ED_{i,\text{CS}}$, in which the MRI score is the integer part of

$$\frac{ED_{i,\text{Normal}}}{ED_{i,\text{Normal}}+ED_{i,CSF}}(r_2 - r_1)+r_1. \qquad \text{(Equation 3)}$$

This standardization allows one to quantitatively compare ISODATA images and evaluate degree of ischemic injury across studies (see Figure 6D). Mitsias et al showed that patients with lower MRI scores were likely to demonstrate at least 20% smaller lesions on follow-up imaging than originally identified on acute ISODATA maps in a study of acute stroke patients seen within 24 h of onset (N=48), with a subset receiving thrombolytic therapy (N=15) [68]. Another study used DWI and normalized ISODATA mismatches in stroke patients (N=45) to predict tissue expansion at 3 months [69]. Other improvements to the ISODATA algorithm include spatial contiguity constraints and use of the Mahalanobis function in place of the Euclidean function for distance metric [70].

## Conclusion

Tissue theme maps have much promise in increasing our understanding of the mechanisms of brain tissue's response to injury and to therapeutic intervention. These maps have the benefit of providing a metric that can be readily translated from pre-clinical lab bench settings to clinical bedside settings. The inherent spatial resolution in tissue theme maps can be used to track the unique evolution of different tissue regions in response to therapies. By being able to identify early on whether a therapy is effective or not, e.g. affecting its expected biologic target, a prospectively determined ineffective treatment can be stopped and replaced with one that may show a response, for example, in the case of brain tumors. Alternatively, theme maps have the potential to noninvasively identify which patients are

NIH-PA Author Manuscript

NIH-PA Author Manuscript

NIH-PA Author Manuscript

most likely to respond to therapeutic intervention, e.g. by demonstrating presence of still salvageable tissue after stroke, thereby improving triage of patients and patient management. Although examples presented here are primarily from the stroke and neuro-oncology field, there is little doubt that similar tissue theme map approaches can be extended to study other brain disorders. Further, continuing advances in both development of new MRI contrasts and algorithms for combining these parameters suggest that the potential of theme maps to assist in the diagnosis and prognosis of brain disorders have only just been broached.

## Acknowledgments

**Sources of Support:**

OW: The author is supported in part by the National Institutes of Health (NIH), grants R01NS59775, R01NS063925, P50NS051343, R01NS051412, R21HL089065 and NCRR [P41RR14075]. The contents of this manuscript are solely the responsibility of the authors and do not necessarily represent the official views of the NIH.

RMD: The author is supported in part through funding from the Royal Netherlands Academy of Arts and Sciences, and the European Union's Seventh Framework Programme (FP7/2007-2013) under grant agreements n° 201024 and n° 202213 (European Stroke Network).

AGS: See http://www.biomarkers.org/pdf/SorensenDisclosures.pdf

The study is supported in part by the National Institutes of Health (NIH), grants R01NS59775, R01NS063925, P50NS051343, R01NS051412, R21HL089065 and NCRR [P41RR14075] and funding from the Royal Netherlands Academy of Arts and Sciences, and the European Union's Seventh Framework Programme (FP7/2007-2013) under grant agreements n° 201024 and n° 202213 (European Stroke Network). The contents of this manuscript are solely the responsibility of the authors and do not necessarily represent the official views of the NIH. The authors would like to thank Robert E Irie for manuscript review.

## References

1. Warach S. Tissue viability thresholds in acute stroke: the 4-factor model. Stroke. 2001; 32(11): 2460–2461. [PubMed: 11692000]
2. Schellinger PD, Fiebach JB, Hacke W. Imaging-based decision making in thrombolytic therapy for ischemic stroke: present status. Stroke. Feb; 2003 34(2):575–583. [PubMed: 12574579]
3. Levine SR. Optimizing an individual's treatment in acute stroke: is a magnetic resonance map leading us towards the holy grail? J Neurol Sci. Nov 15; 2004 225(1–2):1–2. [PubMed: 15465078]
4. Kidwell CS, Alger JR, Saver JL. Beyond mismatch: evolving paradigms in imaging the ischemic penumbra with multimodal magnetic resonance imaging. Stroke. Nov; 2003 34(11):2729–2735. [PubMed: 14576370]
5. Lees KR, Hankey GJ, Hacke W. Design of future acute-stroke treatment trials. Lancet Neurol. Jan; 2003 2(1):54–61. [PubMed: 12849301]
6. Feuerstein GZ, Zaleska MM, Krams M, et al. Missing steps in the STAIR case: a Translational Medicine perspective on the development of NXY-059 for treatment of acute ischemic stroke. J Cereb Blood Flow Metab. Jan; 2008 28(1):217–219. [PubMed: 17579658]
7. Chavez JC, Zaleska MM, Wang X, et al. Multimodal magnetic resonance imaging for assessing evolution of ischemic penumbra: a key translational medicine strategy to manage the risk of developing novel therapies for acute ischemic stroke. J Cereb Blood Flow Metab. Jan; 2009 29(1): 217–219. [PubMed: 18766199]
8. Kucinski T, Naumann D, Knab R, et al. Tissue at risk is overestimated in perfusion-weighted imaging: MR imaging in acute stroke patients without vessel recanalization. AJNR Am J Neuroradiol. Apr; 2005 26(4):815–819. [PubMed: 15814926]
9. Derdeyn CP, Videen TO, Yundt KD, et al. Variability of cerebral blood volume and oxygen extraction: stages of cerebral haemodynamic impairment revisited. Brain. Mar; 2002 125(Pt 3):595–607. [PubMed: 11872616]

NIH-PA Author Manuscript

NIH-PA Author Manuscript

NIH-PA Author Manuscript


10. Schwamm LH, Koroshetz WJ, Sorensen AG, et al. Time course of lesion development in patients with acute stroke: Serial diffusion- and hemodynamic-weighted magnetic resonance imaging. Stroke. 1998; 29:2268–2276. [PubMed: 9804633]
11. Warach S, Li W, Ronthal M, Edelman RR. Acute cerebral ischemia: evaluation with dynamic contrast-enhanced MR imaging and MR angiography. Radiology. Jan; 1992 182(1):41–47. [PubMed: 1727307]
12. Wintermark M, Albers GW, Alger JR, et al. Acute Stroke Imaging Consortium Roadmap. Stroke. 2008; 39(5):1621–1628. Epub 2008 Apr 10. [PubMed: 18403743]
13. Batchelor TT, Sorensen AG, di Tomaso E, et al. AZD2171, a pan-VEGF receptor tyrosine kinase inhibitor, normalizes tumor vasculature and alleviates edema in glioblastoma patients. Cancer Cell. Jan; 2007 11(1):83–95. [PubMed: 17222792]
14. Cutrer FM, Sorensen AG, Weisskoff RM, et al. Perfusion-weighted imaging defects during spontaneous migrainous aura. Ann Neurol. 1998; 43(1):25–31. [PubMed: 9450765]
15. Bakshi R, Thompson AJ, Rocca MA, et al. MRI in multiple sclerosis: current status and future prospects. Lancet Neurol. Jul; 2008 7(7):615–625. [PubMed: 18565455]
16. Fayed N, Davila J, Oliveros A, Castillo J, Medrano JJ. Utility of different MR modalities in mild cognitive impairment and its use as a predictor of conversion to probable dementia. Acad Radiol. Sep; 2008 15(9):1089–1098. [PubMed: 18692749]
17. Viswanathan A, Godin O, Jouvent E, et al. Impact of MRI markers in subcortical vascular dementia: A multi-modal analysis in CADASIL. Neurobiol Aging. Oct 14.2008
18. Bozzao A, Floris R, Baviera ME, Apruzzese A, Simonetti G. Diffusion and perfusion MR imaging in cases of Alzheimer's disease: correlations with cortical atrophy and lesion load. AJNR Am J Neuroradiol. Jun-Jul; 2001 22(6):1030–1036. [PubMed: 11415893]
19. O'Brien TJ, David EP, Kilpatrick CJ, Desmond P, Tress B. Contrast-enhanced perfusion and diffusion MRI accurately lateralize temporal lobe epilepsy: a pilot study. J Clin Neurosci. Sep; 2007 14(9):841–849. [PubMed: 17596947]
20. Szabo K, Poepel A, Pohlmann-Eden B, et al. Diffusion-weighted and perfusion MRI demonstrates parenchymal changes in complex partial status epilepticus. Brain. Jun; 2005 128(Pt 6):1369–1376. [PubMed: 15743871]
21. Nagesh V, Welch KMA, Windham JP, et al. Time course of ADCw changes in ischemic stroke: Beyond the Human Eye! Stroke. 1998; 29:1778–1782. [PubMed: 9731594]
22. Welch KMA, Windham J, Knight RA, et al. A model to predict the histopathology of human stroke using diffusion and T2-weighted magnetic resonance imaging. Stroke. 1995; 26(11):1983–1989. [PubMed: 7482635]
23. D'Olhaberriague L, Welch KMA, Nagesh V, et al. Preliminary clinical-radiological assessment of a MR tissue sigature model in human stroke. J Neurol Sci. 1998; 156:158–166. [PubMed: 9588851]
24. Schlaug G, Benfield A, Baird AE, et al. The ischemic penumbra: operationally defined by diffusion and perfusion MRI. Neurology. 1999; 53(7):1528–1537. [PubMed: 10534263]
25. Neumann-Haefelin T, Wittsack HJ, Wenserski F, et al. Diffusion- and perfusion-weighted MRI. The DWI/PWI mismatch region in acute stroke. Stroke. 1999; 30(8):1591–1597. [PubMed: 10436106]
26. Parsons MW, Yang Q, Barber PA, et al. Perfusion magnetic resonance imaging maps in hyperacute stroke : relative cerebral blood flow most accurately identifies tissue destined to infarct. Stroke. 2001; 32(7):1581–1587. [PubMed: 11441205]
27. Baird AE, Warach S. Magnetic resonance imaging of acute stroke. J Cereb Blood Flow Metab. 1998; 18(6):583–609. [PubMed: 9626183]
28. Sorensen AG, Buonanno FS, Gonzalez RG, et al. Hyperacute stroke: Evaluation with combined multisection diffusion-weighted and hemodynamically weighted echo-planar MR imaging. Radiology. 1996; 199:391–401. [PubMed: 8668784]
29. Fisher M. Recommendations for advancing development of acute stroke therapies: Stroke Therapy Academic Industry Roundtable 3. Stroke. Jun; 2003 34(6):1539–1546. [PubMed: 12750546]
30. Muir KW. Heterogeneity of stroke pathophysiology and neuroprotective clinical trial design. Stroke. Jun; 2002 33(6):1545–1550. [PubMed: 12052989]

NIH-PA Author Manuscript

NIH-PA Author Manuscript

NIH-PA Author Manuscript


31. Menezes NM, Ay H, Wang Zhu M, et al. The real estate factor: quantifying the impact of infarct location on stroke severity. Stroke. Jan; 2007 38(1):194–197. [PubMed: 17122428]
32. Collins DL, Neelin P, Peters TM, Evans AC. Automatic 3D intersubject registration of MR volumetric data in standardized Talairach space. J Comput Assist Tomogr. Mar-Apr; 1994 18(2): 192–205. [PubMed: 8126267]
33. Jenkinson M, Smith S. A global optimisation method for robust affine registration of brain images. Med Image Anal. Jun; 2001 5(2):143–156. [PubMed: 11516708]
34. Jenkinson M, Bannister P, Brady M, Smith S. Improved optimization for the robust and accurate linear registration and motion correction of brain images. Neuroimage. 2002; 17(2):825–841. [PubMed: 12377157]
35. Woods RP, Cherry SR, Mazziotta JC. Rapid automated algorithm for aligning and reslicing PET images. J Comput Assist Tomogr. 1992; 16(4):620–633. [PubMed: 1629424]
36. Woods RP, Grafton ST, Holmes CJ, Cherry SR, Mazziotta JC. Automated image registration: I. General methods and intrasubject, intramodality validation. J Comput Assist Tomogr. 1998; 22(1): 139–152. [PubMed: 9448779]
37. van der Kouwe AJ, Benner T, Fischl B, et al. On-line automatic slice positioning for brain MR imaging. Neuroimage. Aug 1; 2005 27(1):222–230. [PubMed: 15886023]
38. Benner T, Wisco JJ, van der Kouwe AJ, et al. Comparison of manual and automatic section positioning of brain MR images. Radiology. Apr; 2006 239(1):246–254. [PubMed: 16507753]
39. Duda, RO.; Hart, PE.; Stork, DG. Pattern Classification. 2. New York: John Wiley & Sons, Inc; 2001.
40. Bishop, CM. Neural Networks for Pattern Recognition. New York: Oxford University Press Inc; 1995.
41. Knight RA, Dereski MO, Helpern JA, Ordidge RJ, Chopp M. Magnetic resonance imaging assessment of evolving focal cerebral ischemia. Comparison with histopathology in rats. Stroke. 1994; 25(6):1252–1261. [PubMed: 8202989]
42. Pierpaoli C, Righini A, Linfante I, Tao-Cheng JH, Alger JR, Di Chiro G. Histopathologic correlates of abnormal water diffusion in cerebral ischemia: diffusion-weighted MR imaging and light and electron microscopic study. Radiology. Nov; 1993 189(2):439–448. [PubMed: 8210373]
43. Moffat BA, Chenevert TL, Lawrence TS, et al. Functional diffusion map: a noninvasive MRI biomarker for early stratification of clinical brain tumor response. Proc Natl Acad Sci U S A. Apr 12; 2005 102(15):5524–5529. [PubMed: 15805192]
44. Hamstra DA, Galban CJ, Meyer CR, et al. Functional diffusion map as an early imaging biomarker for high-grade glioma: correlation with conventional radiologic response and overall survival. J Clin Oncol. Jul 10; 2008 26(20):3387–3394. [PubMed: 18541899]
45. Galban CJ, Chenevert TL, Meyer CR, et al. The parametric response map is an imaging biomarker for early cancer treatment outcome. Nat Med. May; 2009 15(5):572–576. [PubMed: 19377487]
46. Waldman AD, Jackson A, Price SJ, et al. Quantitative imaging biomarkers in neuro-oncology. Nat Rev Clin Oncol. Aug; 2009 6(8):445–454. [PubMed: 19546864]
47. Wu O, Koroshetz WJ, Østergaard L, et al. Predicting tissue outcome in acute human cerebral ischemia using combined diffusion- and perfusion-weighted MR imaging. Stroke. 2001; 32(4): 933–942. [PubMed: 11283394]
48. Efron, B. The Jackknife, the bootstrap and other resampling plans. Philadelphia: Society for Industrial and Applied Mathematics; 1982.
49. Wu, O.; Koroshetz, WJ.; Gonzalez, RG., et al. Effects of MR perfusion parameters selection on the prediction of tissue infarction in acute human stroke (abstr). Paper presented at: ISMRM Fourteenth Scientific Meeting; May 6–12, 2006; Seattle, WA.
50. Wu O, Christensen S, Hjort N, et al. Characterizing physiological heterogeneity of infarction risk in acute human ischaemic stroke using MRI. Brain. Sep; 2006 129(Pt 9):2384–2393. [PubMed: 16891322]
51. Sorensen AG, Copen WA, Østergaard L, et al. Hyperacute stroke: simultaneous measurement of relative cerebral blood volume, relative cerebral blood flow, and mean tissue transit time. Radiology. 1999; 210(2):519–527. [PubMed: 10207439]
52. Hastie, T.; Tibshirani, RJ. Generalized Additive Models. New York: Chapman and Hall; 1990.

NIH-PA Author Manuscript

NIH-PA Author Manuscript

NIH-PA Author Manuscript


53. Wu, O.; Koroshetz, WJ.; Østergaard, L., et al. Extension of MRI-Based Predictive Models of Infarction in Hyperacute Human Cerebral Ischemia (abstr). Paper presented at: ISMRM Seventh Scientific Meeting; May 24–28, 1999; Philadelphia, PA.
54. McLachan, GJ.; Basford, KE. Mixture models: inference and application to clustering. New York: Marcel Dekker; 1998.
55. Rose SE, Chalk JB, Griffin MP, et al. MRI based diffusion and perfusion predictive model to estimate stroke evolution. Magn Reson Imaging. 2001; 19(8):1043–1053. [PubMed: 11711228]
56. Carano RA, Takano K, Helmer KG, et al. Determination of focal ischemic lesion volume in the rat brain using multispectral analysis. J Magn Reson Imaging. Nov-Dec; 1998 8(6):1266–1278. [PubMed: 9848739]
57. Jordan MI, Jacobs RA. Hierarchical mixtures of experts and the EM algorithm. Neural Comput. 1994; 6:181–214.
58. Wu, O.; Koroshetz, WJ.; Østergaard, L., et al. Predicting tissue infarction in hyperacute human cerebral ischemia using a hierarchical mixture of experts (abstr). Paper presented at: ISMRM Tenth Scientific Meeting; May 18–24, 2002; Honolulu, HI. 2002.
59. Gottrup C, Thomsen K, Locht P, et al. Applying instance-based techniques to prediction of final outcome in acute stroke. Artif Intell Med. Mar; 2005 33(3):223–236. [PubMed: 15811787]
60. Lee MC, Nelson SJ. Supervised pattern recognition for the prediction of contrast-enhancement appearance in brain tumors from multivariate magnetic resonance imaging and spectroscopy. Artif Intell Med. May; 2008 43(1):61–74. [PubMed: 18448318]
61. Carano RA, Li F, Irie K, et al. Multispectral analysis of the temporal evolution of cerebral ischemia in the rat brain. J Magn Reson Imaging. 2000; 12(6):842–858. [PubMed: 11105022]
62. Srinivasan A, Galban CJ, Johnson TD, Chenevert TL, Ross BD, Mukherji SK. Utility of the K-Means Clustering Algorithm in Differentiating Apparent Diffusion Coefficient Values of Benign and Malignant Neck Pathologies. AJNR Am J Neuroradiol. Dec 10.2009
63. Ball GH, Hall DJ. A clustering technique for summarizing multivariate data. Behav Sci. Mar; 1967 12(2):153–155. [PubMed: 6030099]
64. Bezdek JC. A Convergence Theorem for the Fuzzy ISODATA Clustering Algorithms. IEEE Transactions on Pattern Analysis and Machine Intelligence. 1980; PAMI-2(1):1–8.
65. Jacobs MA, Mitsias P, Soltanian-Zadeh H, et al. Multiparametric MRI tissue characterization in clinical stroke with correlation to clinical outcome: Part 2. Stroke. 2001; 32(4):950–957. [PubMed: 11283396]
66. Mitsias PD, Jacobs MA, Hammoud R, et al. Multiparametric MRI ISODATA ischemic lesion analysis: correlation with the clinical neurological deficit and single-parameter MRI techniques. Stroke. 2002; 33(12):2839–2844. [PubMed: 12468779]
67. Soltanian-Zadeh H, Pasnoor M, Hammoud R, et al. MRI tissue characterization of experimental cerebral ischemia in rat. J Magn Reson Imaging. Apr; 2003 17(4):398–409. [PubMed: 12655578]
68. Mitsias PD, Ewing JR, Lu M, et al. Multiparametric iterative self-organizing MR imaging data analysis technique for assessment of tissue viability in acute cerebral ischemia. AJNR Am J Neuroradiol. Oct; 2004 25(9):1499–1508. [PubMed: 15502128]
69. Lu M, Mitsias PD, Ewing JR, et al. Predicting final infarct size using acute and subacute multiparametric MRI measurements in patients with ischemic stroke. J Magn Reson Imaging. May; 2005 21(5):495–502. [PubMed: 15834917]
70. Shen Q, Ren H, Fisher M, Bouley J, Duong TQ. Dynamic tracking of acute ischemic tissue fates using improved unsupervised ISODATA analysis of high-resolution quantitative perfusion and diffusion data. J Cereb Blood Flow Metab. Sep; 2004 24(8):887–897. [PubMed: 15362719]

NIH-PA Author Manuscript

NIH-PA Author Manuscript

NIH-PA Author Manuscript

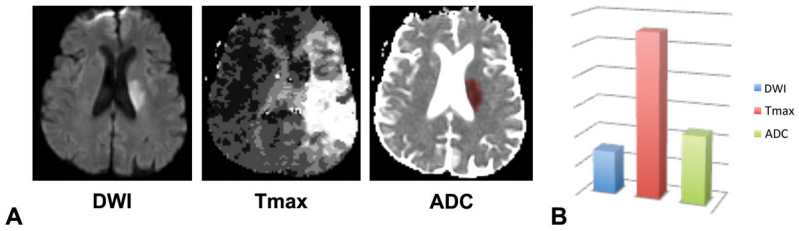


**Figure 1.**
Multimodal MRI: Volumetric Analysis. An example of volumetric analysis of multimodal MRI consisting of acute (A) DWI, Tmax and ADC from a single stroke patient, where for statistical analysis (B) one can compare lesion volumes.

NIH-PA Author Manuscript

NIH-PA Author Manuscript

NIH-PA Author Manuscript

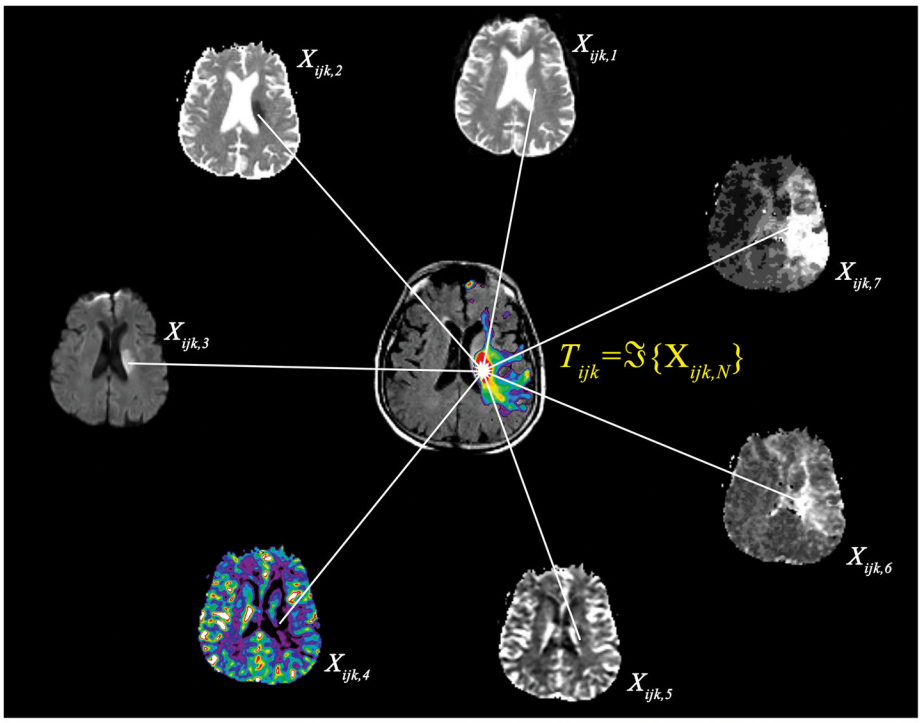


**Figure 2.**

Multimodal MRI: Voxel-based Tissue Theme Maps. In a voxel-based approach, one transforms quantitative imaging values for each voxel <i,j,k> from each parametric map, $X_{ijk,1\ldots N}$, to create a single new imaging map $T$, where the value at each voxel <i,j,k> is a function, $\Im$, of N imaging parameters, where in this example, N=7. This function may either be a linear or non-linear.

NIH-PA Author Manuscript

NIH-PA Author Manuscript

NIH-PA Author Manuscript

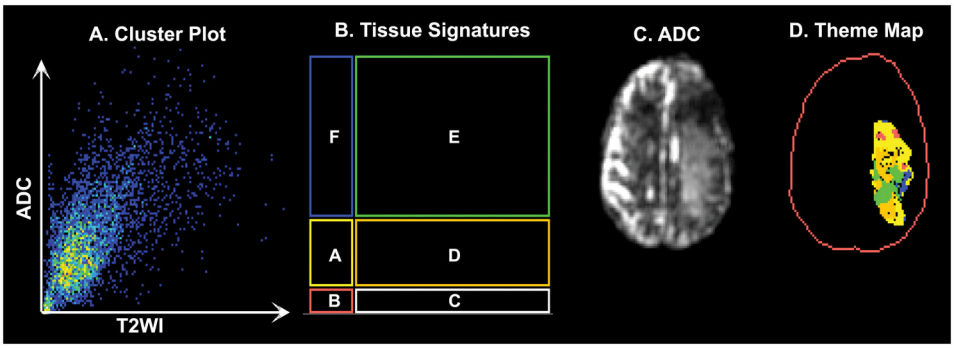


**Figure 3.**

Example of (A) cluster plot, (B) tissue signatures, (C) ADC map and (D) derived theme map for a stroke patient using ADC and T2WI data. Signature A represents normal tissue, while classes B–F represent tissue at different stages of injury. Courtesy of Dr. K. Michael Welch.

NIH-PA Author Manuscript

NIH-PA Author Manuscript

NIH-PA Author Manuscript

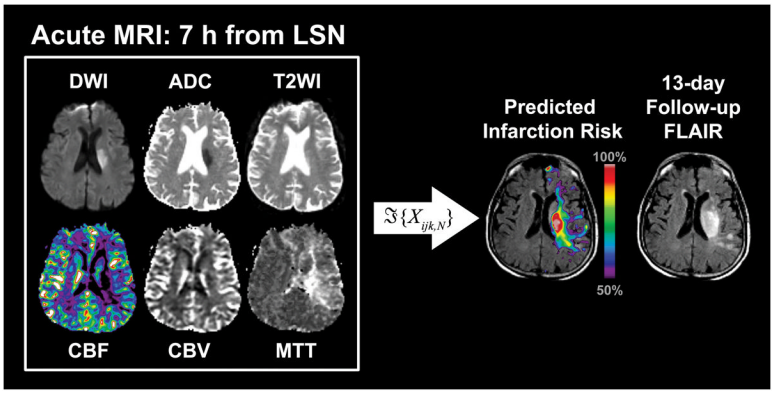


**Figure 4.**

Example input and output for a GLM using acute MRI data from a stroke patient imaged within 7 h since last seen normal (LSN). Here six imaging parameters were combined on a voxel-wise basis using a GLM algorithm where the coefficients were derived from other stroke patients. The predicted infarction risk map is overlaid on the follow-up FLAIR data, with only tissue with greater than 50% likelihood of infarction shown for clarity purposes. Note that the amount of tissue with more than 50% chance of becoming infarcted corresponds spatially well with actual outcome at 13 days.

NIH-PA Author Manuscript

NIH-PA Author Manuscript

NIH-PA Author Manuscript

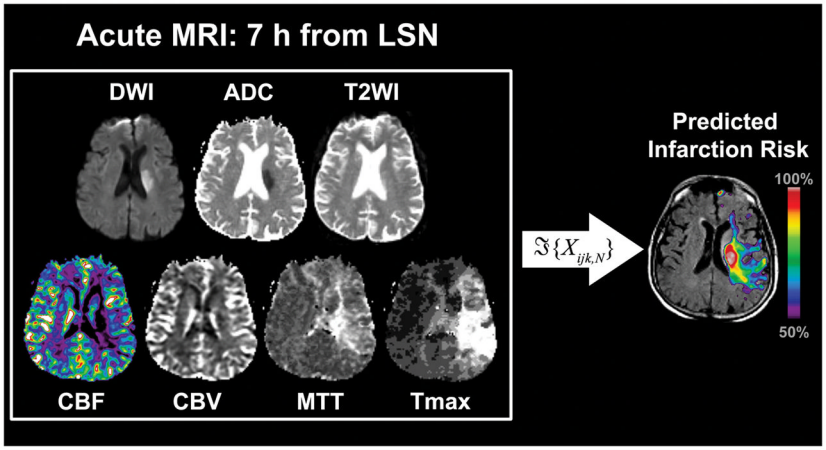


**Figure 5.**
Effect of adding additional imaging parameters on output of GLM algorithms. An additional parameter was added to the model shown in Figure 4, generating an infarction risk map that can be interpreted in the same fashion as the simpler 6-parameter model. Although the Tmax map demarcates a large region of abnormality, the GLM output appears similar to Figure 4, with slightly less false positives in normal parenchyma on the 13-day FLAIR.

NIH-PA Author Manuscript

NIH-PA Author Manuscript

NIH-PA Author Manuscript

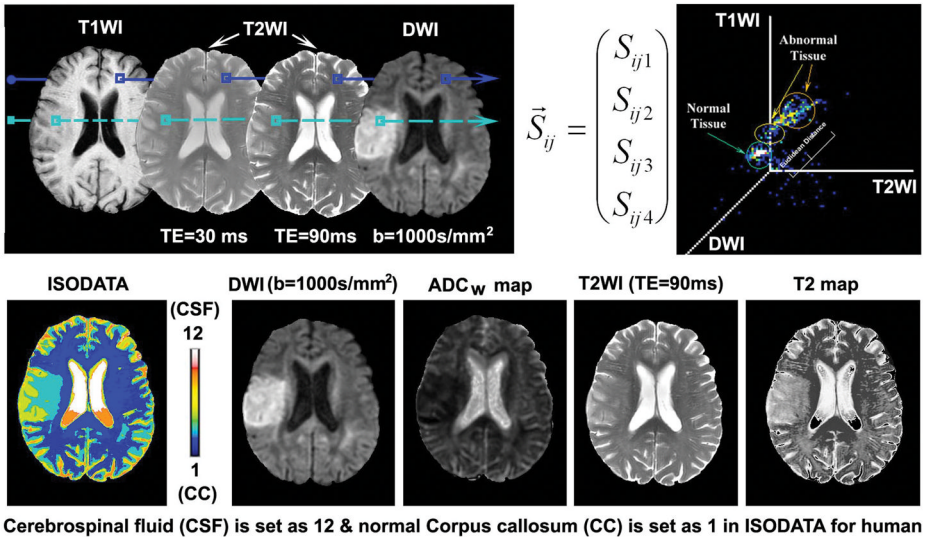


**Figure 6.**

Illustration of the multiparametric ISODATA segmentation. (A) Four MRI images (1 T1WI, 2 T2WI with TE=30 and 90 ms, 1 DWI with b=1000s/mm$^2$) are coregistered, warped and inputted for the ISODATA algorithm. (B) The tissue signature vector is a mathematical descriptor, and defined as $S_{ij}$=[$S_{ij1}$,Sij2, $S_{ij3}$, $S_{ij4}$], where $S_{ijk}$ is the k-th element of the ij-th pixel vector, i.e., the mean gray level of the ij-th pixel in the k-th image in the image sequence. (C) A representation of the 3-dimensional feature space formed by T1WI, T2WI and DWI (the 3-dimensional feature space is shown for easy visualization). The Euclidean distance model is demonstrated with the distribution of tissue clusters in the 3-dimensional feature space. The Euclidean distances are calculated between the normal tissue and abnormal tissue clusters using each cluster's tissue signature vector. Each axis represents the signal intensity distribution for each MR image. (D) A multiparametric ISODATA theme map clearly demonstrates heterogeneous regions within the lesion. These different areas of tissue damage are visualized with indices from 1 (assigned to normal corpus callosum) to 12 (assigned to cerebrospinal fluid). The corresponding MRI images are, (E) a DWI image with b=1000s/mm$^2$, (F) an $ADC_w$ map, (G) a T2WI image with TE=90 ms and (H) a $T_2$ map. Courtesy of Dr. Michael Chopp, Dr. Gary Ding and Dr. Quan Jiang.